Modeled Variations of Precipitation over the Greenland Ice Sheet@

DAVID H. BROMWICH,*,† FRANK M. ROBASKY,* RICHARD A. KEEN,** AND JOHN F. BOLZAN*,‡

*Byrd Polar Research Center, The Ohio State University, Columbus, Ohio
†Atmospheric Sciences Program, The Ohio State University, Columbus, Ohio
**Golden, Colorado
‡Department of Geological Sciences, The Ohio State University, Columbus, Ohio

(Manuscript received 11 February 1992 in final form 28 January 1993)

ABSTRACT

A parameterization of the synoptic activity at 500 hPa and a simple orographic scheme are used to model the spatial and temporal variations of precipitation over the Greenland Ice Sheet for 1963–88 from analyzed geopotential height fields produced by the National Meteorological Center (NMC). Model coefficients are fitted to observed accumulation data, primarily from the summit area of the ice sheet. All major spatial characteristics of the observed accumulation distribution are reproduced apart from the orographic accumulation maximum over the northwestern coastal slopes. The modeled time-averaged total precipitation amount over Greenland is within the range of values determined by other investigators from surface-based observations. A realistic degree of interannual variability in precipitation is also simulated.

A downward trend in simulated ice sheet precipitation over the 26 years is found. This is supported by a number of lines of evidence. It matches the accumulation trends during this period from ice cores drilled in south-central Greenland. The lower tropospheric specific humidities at two south coastal radiosonde stations also decrease over this interval. A systematic shift away from Greenland and a decrease in activity of the dominant storm track are found for relatively low precipitation periods as compared to relatively high precipitation periods. This negative precipitation trend would mean that the Greenland Ice Sheet, depending on its 1963 mass balance state, has over the 1963–88 period either decreased its negative, or increased its positive, contribution to recently observed global sea level rise.

Superimposed on the declining simulated precipitation rate for the entire ice sheet is a pronounced 3–5-yr periodicity. This is prominent in the observed and modeled precipitation time series from Summit, Greenland. This cycle shows some aspects in common with the Southern Oscillation.

Some deficiencies in the NMC analyses were highlighted by this work. A large jump in simulated precipitation amounts at Summit around 1962, which is not verified by accumulation data, is inferred to be due to an artificial increase in cyclonic activity at 500 hPa associated with the NMC change from manual to numerical analyses. The activity of the storm track along the west coast of Greenland appears to be anomalously low in the NMC analyses, perhaps due to mesoscale cyclogenesis that is not resolved by the NMC analysis scheme.

1. Introduction

The Greenland Ice Sheet presents an anomalous situation with regard to meteorological and glaciological investigations. Some of the most important climatic records addressing the cause(s) of the transition from the last glacial (Wisconsinan) age to the present interglacial (Holocene) have been extracted from ice cores drilled from the ice sheet (Langway et al. 1985). Currently, major efforts by investigators from the United States (GISP 2) and Europe (GRIP) are under way to extract more detailed and longer-time ice-core records from the summit region of the ice sheet (Commission for Scientific Research in Greenland 1989; Johnsen et al. 1992). From a meteorological point of view, however, the Greenland Ice Sheet is one of the least studied areas in the Northern Hemisphere. Abundant measurements are available from the populated, ice-free, coastal areas but only scattered sites have been occupied, generally intermittently, on the ice sheet proper (Putnins 1970). This situation is starting to change with detailed reevaluations of existing datasets (e.g., Ohmura 1987; Ohmura and Reeh 1991), examinations of satellite imagery (Scorer 1988; Rasmussen 1989), and the recent deployments of, and results from, automatic weather stations (Stearns and Weidner 1991; Weidner and Stearns 1991). This paper addresses an important aspect of Greenland Ice Sheet meteorology, namely, precipitation variations over the last two-and-a-half decades. Studies of interannual precipitation variations and stable isotope characteristics of snowfall (e.g., Johnsen et al. 1989) provide complementary results to assist with the interpretation of climatic records from ice cores.

The amount of ice contained by the Greenland Ice Sheet is directly related to global sea level, which appears to be rising at the rate of about 2 mm yr^{-1} (Peltier

@ Contribution 811 of Byrd Polar Research Center.

Corresponding author address: Dr. David H. Bromwich, Byrd Polar Research Center, Ohio State University, 108 Scott Hall, 1090 Carmack Rd., Columbus, OH 43210-1002.

and Tushingham 1989; Douglas 1991). The first measurements of ice sheet elevation change by satellite altimetry suggest that the Greenland surface elevation south of 72°N increased by about 0.20 m yr^{-1} between 1978 and 1986 (Zwally et al. 1989). Although there has been debate about the methodology used to obtain the elevation changes (Douglas et al. 1990; Zwally et al. 1990; Van der Veen 1993), Zwally (1989) interprets this apparent elevation increase as being due to a 25%–45% excess of average ice accumulation over the amount required to balance outward ice flow. The implied global sea level depletion is 0.20 to 0.41 mm yr^{-1}, depending on whether the thickening is caused by shorter- (5–10 yr) or longer- (<100 yr) term changes. If a similar discrepancy exists in the northern 60% of the ice sheet then the global depletion rate is 75% larger than the aforementioned values. Zwally suggested that the increased ice thickness might be caused by recent precipitation increases associated with generally higher Arctic temperatures this century (e.g., Kelly et al. 1982). Clearly, a systematic evaluation of the precipitation trends over Greenland is one of the components needed to assess the validity of Zwally's dramatic findings.

Studies suggest substantial spatial variability in Greenland precipitation (accumulation) trends over the last 30–40 years. (Precipitation is nearly equal to net snow accumulation over the interior of the ice sheet.) Keen (1984, see his Fig. 6), using a precipitation model that is the subject of this paper, obtained generally decreasing amounts over northwestern Greenland and increasing amounts over west-central Greenland. Ice-core results presented by Clausen et al. (1988) showed accumulation decreases in central Greenland over the latter half of the twentieth century. Bolzan and Strobel (1993) found, also from ice-core analyses, no discernible accumulation trend for 1959–86 near the ice sheet summit. Such variability in space and time is the key factor limiting evaluations of the ice budget in Greenland (Kostecka and Whillans 1988).

Decadal precipitation variability is also to be expected from studies of the large-scale atmospheric circulation. There are substantial changes in cyclonic activity on these time scales (Keen 1980) as well as in associated circulation types (van Loon and Rogers 1978). Such changes are known to be associated with variations in Greenland precipitation amounts (Rogers and van Loon 1979).

This study uses a modified version of the statistical–dynamical model by Keen (1984) to simulate precipitation variability over Greenland during the last two-and-a-half decades. Precipitation is parameterized in terms of short-wave positive vorticity advection at 500 hPa diagnosed from 500-hPa geopotential height analyses produced by the National Meteorological Center (NMC). A more detailed description of the model than given by Keen (1984) is presented in section 2, along with the modifications implemented in the present investigation. The method used to infer empirical coefficients from observed accumulation time series is also outlined. This is followed by a discussion of the spatial and temporal variations of modeled precipitation amounts. The final section evaluates the findings and the impact of analysis changes implemented by NMC and explores some implications of the results.

2. Methods

The precipitation falling at a certain point and time is computed as

$$P = A_0 q_{700} |\mathrm{VFI}| + A_1 q_{700} \mathbf{V}_{850} \cdot \nabla H \qquad (1)$$

where A_0 and A_1 are empirically derived coefficients, q_{700} is the climatological specific humidity at the 700-hPa level for the month in question, VFI is the "vorticity flux index" (to be explained below), $\mathbf{V}_{850}$ is the geostrophic velocity at the 850-hPa level, and H is the terrain height of the Greenland Ice Sheet. The first term on the right-hand side will be referred to as the "dynamic" component of the model as it simulates precipitation due to synoptic-scale cyclonic disturbances. The second right-hand side term will be referred to as the "orographic" component as it simulates precipitation due to the forced uplift of air over the topography of Greenland. In the following subsections the input data used and the derivation and implementation of (1) will be discussed.

a. Data

The basic input datasets used were 1200 UTC gridded Northern Hemispheric geopotential height analyses at the 500- and 850-hPa levels produced by NMC and obtained on CD-ROM from the National Center for Atmospheric Research (NCAR). Although the 500-hPa geopotential height data were available for 1 January 1946 through 30 June 1989, only the data after 1 January 1963 were used. This was due to (i) the questionable nature of the analyses for the 1946–63 period, to be discussed in section 4b, and (ii) the 850-hPa heights that were only available for 1963–89. The polar stereographic grid for these data has a spacing that varies with latitude, ranging from 306 km at 30°N to 408 km at the North Pole (Jenne 1970). The original computational grid in the Greenland area used for this model is shown in Fig. 1.

Climatological monthly mean specific humidities at the 700-hPa level were computed from climatological monthly mean dewpoints at this same level. The latter were gridded from the analyses of Crutcher and Meserve (1970).

Greenland Ice Sheet terrain heights employed are those used by Radok et al. (1982) and made available in a digitized form with a 20-km grid spacing by the National Snow and Ice Data Center (NSIDC). These elevations are shown in Fig. 2.

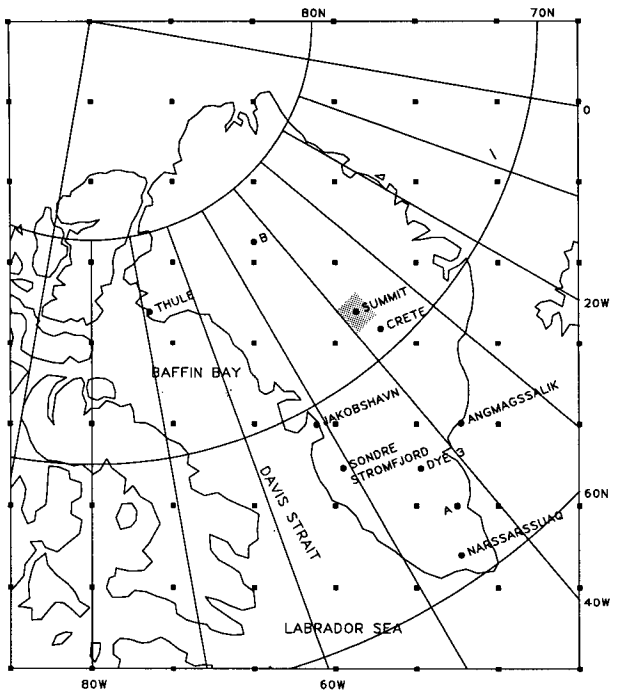

FIG. 1. Computational grid (filled squares) and location map of the Greenland neighborhood. The shaded area labeled Summit marks the region of critical accumulation data. The letters "A" and "B" are grid points for which calculation results are provided in Figs. 11 and 14.

b. *Dynamic component*

1) VORTICITY FLUX INDEX

The vorticity flux index (VFI) serves as our parameterization of vertical velocity due to synoptic-scale cyclone activity. It is based on the equivalent barotropic model of the atmosphere (Charney 1949). [The appropriateness of the equivalent barotropic assumption is discussed in section 2b(3).] In such a model of the atmosphere, it can be shown that (Haltiner 1971)

$$\omega = p_0 f^{-1} C(p) \mathbf{V}^* \cdot \nabla \zeta^* + B(p)\omega_0. \quad (2)$$

In this equation, asterisks indicate the integral mean with respect to pressure through the entire depth of the troposphere, ω is the vertical velocity in pressure coordinates, p_0 and ω_0 are surface values of pressure and vertical velocity, respectively, f is the Coriolis parameter, $\mathbf{V}$ is the horizontal wind vector, and ζ is the relative vorticity. Here $B(p)$ and $C(p)$ are slowly varying nondimensional functions of pressure based on the vertical shear of the wind speed. The first right-hand side term of (2) calculates dynamically induced ω, with $C(p)$ based on climatological data yielding maximum vertical velocities from this term near the middle troposphere (near the 500-hPa level) with upward (downward) vertical motions associated with positive (negative) vorticity advection. The second term on the right-hand side of (2) is the contribution to ω due to the lower boundary; it will be simulated through the orographic component of the precipitation model.

The equivalent barotropic assumption holds that the horizontal motion fields of the model atmosphere correspond to those of the actual atmosphere at one level, called the equivalent barotropic level. This has been found to be near the 500-hPa level. If calculations are made on this equivalent barotropic level, then $\mathbf{V} \cdot \nabla \zeta$ at that level may be substituted for $\mathbf{V}^* \cdot \nabla \zeta^*$ in (2). Recall that it is near this level that $C(p)$ is maximized as well.

The geostrophic wind and vorticity are calculated in such a way as to emphasize the advection of "short-wave" vorticity by the "long-wave" wind field. This is in an attempt to capture the motion and intensity of the baroclinic short waves embedded in the long-wave flow, which likely are responsible for the majority of Greenland's precipitation. We begin by computing the geostrophic relative vorticity at the 500-hPa level using the centered finite-difference expression

$$\zeta = \frac{g}{f}\nabla^2 Z \approx -\frac{g}{d^2 f}(Z - \bar{Z}) \equiv -\frac{g}{d^2 f} Z', \quad (3)$$

where $\bar{Z}$ is the spatially smoothed geopotential field defined at grid point (i, j) by

$$\bar{Z}_{i,j} \equiv \frac{1}{4}(Z_{i+2,j} + Z_{i-2,j} + Z_{i,j+2} + Z_{i,j-2}), \quad (4)$$

and Z' is the difference between the original height

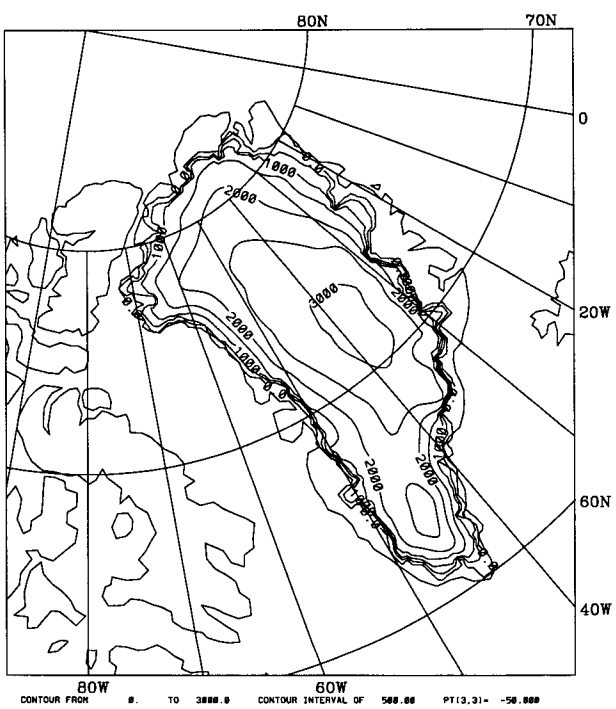

FIG. 2. High-resolution terrain (20 km) used for the orographic precipitation calculations. The contouring interval is 500 m.

field and the spatially smoothed field. In a similar fashion, a long-wave relative vorticity $\bar{\zeta}$ can be computed as

$$\bar{\zeta} = \frac{g}{f}\nabla^2\bar{Z} \approx -\frac{g}{d^2 f}(\bar{Z} - \bar{\bar{Z}}), \tag{5}$$

where $\bar{\bar{Z}}$ is computed by twice applying (4) to the height field. The short-wave relative vorticity is then defined and computed as

$$\zeta' \equiv \zeta - \bar{\zeta}. \tag{6}$$

This is, in effect, a bandpass filter emphasizing vorticity features near 2400-km wavelength (six times the NMC grid spacing, or $6d$) and suppressing the shorter wavelengths (3–$4d$) that are most sensitive to changes in NMC's analysis procedures (Wahl 1972). (Wavelengths less than $3d$ are suppressed by the NMC analysis scheme.) The long-wave 500-hPa geostrophic wind field is then computed as

$$\bar{\mathbf{V}} = \frac{g}{f}\mathbf{k} \times \nabla\bar{Z} \approx -\frac{g}{f}\left[\frac{\bar{Z}_{i,j+2} - \bar{Z}_{i,j-2}}{4d}\mathbf{i} + \frac{\bar{Z}_{i+2,j} - \bar{Z}_{i-2,j}}{4d}\mathbf{j}\right]. \tag{7}$$

It can be shown that, if the geostrophic wind is partitioned into long- and short-wave constituents similar to what was done for ζ in (6), only this long-wave geostrophic wind field (7) is effective in advecting geostrophic relative vorticity. Here $\bar{\mathbf{V}}$ retains wavelengths longer than $10d$ at more than 0.5 full amplitude. Because 500 hPa is near the level of nondivergence, $\bar{\mathbf{V}}$ closely approximates the actual displacement field of the short-wave vorticity (Fjortoft 1952). This is consistent with the concept of "steering" discussed by Godske et al. (1957) and Palmén and Newton (1969) and useful to forecasters.

To simplify the computations by eliminating the need to take higher-order derivatives (beyond that required to calculate the velocity and relative vorticity), we take the advection of short-wave geostrophic relative vorticity by the long-wave wind field to be directly proportional to the flux quantity $\bar{\mathbf{V}}\zeta'$. This assumption presumes that we are calculating at the level of nondivergence, that the short waves are sinusoidal, and that their aggregate mean length does not vary significantly with time or location. Thus, the vorticity flux index (VFI) for a certain time is defined as

$$\text{VFI} \equiv \bar{\mathbf{V}}\zeta'' \quad \begin{Bmatrix} \zeta'' = \zeta', & \zeta' \geq 0 \\ \zeta'' = 0, & \zeta' < 0 \end{Bmatrix}, \tag{8}$$

the magnitude of which will be taken as our parameterization of vertical velocity resulting from synoptic-scale forcing. As we are only interested in upward motion and the resulting precipitation, only positive relative vorticity is considered in (8). The mean daily VFI for the period 1963–89 is shown in Fig. 3. Note that the upper-level disturbances approach Greenland, in the mean, from the west and southwest and that the intensity, and/or frequency of these disturbances is greatest along the southeast coast, near the mean position of the semipermanent Icelandic Low.

As precipitation is directly proportional to the moisture content of the atmosphere as well as to the amount of vertical motion, |VFI| is multiplied by the specific humidity at the 700-hPa level. This level was chosen because any lower level would largely lie underneath the Greenland Ice Sheet (see Fig. 2) while any higher level would not capture the moisture content of the lower troposphere, where most of the atmospheric moisture is concentrated.

2) Empirical coefficient A_0

The product $q_{700}|\text{VFI}|$ is multiplied by a coefficient A_0 in order to allow this product to yield realistic values of precipitation (in cm of water equivalent, or cm w.e.). This coefficient is determined by linear regression of annual values of $q_{700}|\text{VFI}|$ against actual annual accumulation values from the summit area of the ice sheet. These accumulation values were gathered by Bolzan and Strobel (1993), who inferred annual accumulation rates from shallow ice cores taken at nine sites distributed on a 150-km × 150-km survey grid centered on Summit station in central Greenland (the shaded area in Fig. 1). From these data, Bolzan and Strobel (1993) calculated annual accumulation rates

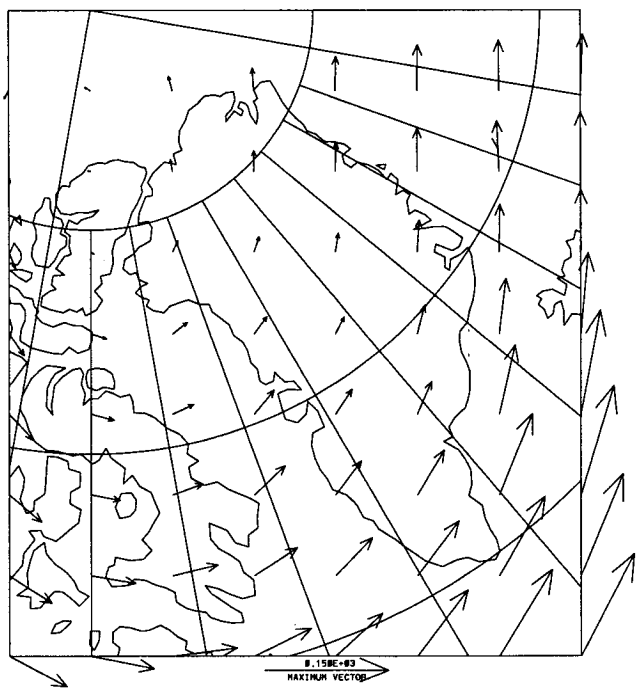

FIG. 3. The mean daily vorticity flux index vectors for 1963–1989. The vector magnitudes have units of meters per second squared.

for 1964–86 averaged over the entire survey grid using all nine ice cores, which we take to be equivalent to the yearly accumulation values at the center of this grid (i.e., Summit station, see Fig. 1). The product $q_{700}|\mathrm{VFI}|$ for Summit was determined by linear interpolation from the four nearest NMC grid points.

Summit station sits very near to the crest of the ice sheet, where terrain height gradients are very small in comparison with those near the coast (Fig. 2). This, and the location of Summit far inland, led to the treatment of all the accumulation at this site as being due to the dynamic component of the model. The slope of the regression line (specified with an intercept of zero) was well determined and yielded a coefficient value of $A_0 = 1.79 \times 10^6$ cm w.e. $\mathrm{m}^{-1}\ \mathrm{s}^2$. Figure 4 shows the time series of annual accumulation from Summit compared to the modeled dynamic precipitation (after the application of A_0). Aside from major discrepancies for 1967 and 1977–79, the model appears to do an adequate job of simulating the magnitude and year-to-year variability of precipitation at this location. When evaluating this comparison, it should be remembered that the two time series are of vastly different origin and horizontal resolution: essentially point glaciological data versus an atmospheric parameterization interpolated from roughly a 400-km grid. In such a case it is not at all clear exactly what degree of interannual correspondence should be expected.

3) VFI VERSUS QUASIGEOSTROPHIC OMEGA

The equivalent barotropic basis of the dynamic component of the precipitation model has been established. The question naturally arises, however, as to the role that baroclinicity plays in the individual cyclonic systems that affect Greenland. Although Blackmon et al. (1979) indicated that the structure of the atmosphere is primarily equivalent barotropic over the central and eastern North Atlantic, this appeared to be more the case for monthly mean data as opposed to the daily time scale. Lau (1979) also indicated that transient wintertime disturbances have a more barotropic structure over the eastern, as opposed to the western, North Atlantic but primarily for areas east of Greenland. The impact of baroclinicity was evaluated using the traditional quasigeostrophic omega equation (e.g., Holton 1992):

$$\left(\nabla^2 + \frac{f_0^2}{\sigma}\frac{\partial^2}{\partial p^2}\right)\omega = \frac{f_0}{\sigma}\frac{\partial}{\partial p}\left[\mathbf{V}_g \cdot \nabla\left(\frac{1}{f_0}\nabla^2\Phi + f\right)\right] + \frac{1}{\sigma}\nabla^2\left[\mathbf{V}_g \cdot \nabla\left(-\frac{\partial\Phi}{\partial p}\right)\right] \quad (9)$$

where σ is the static stability parameter and Φ is the geopotential. In particular, this question can be addressed by determining whether or not the thickness advection [or thermal advection, the second right-hand side term in (9)] is sufficiently small. Calculations using the thermal advection term in (9) indicated that this term was often significant, so an attempt was made to base the dynamic component of the precipitation model on (9). This was done by assuming that the left-hand side of (9) is directly proportional to $-\omega$ (or to w, the vertical velocity in z coordinates). The right-hand side of (9), with σ assumed constant and factored out, was calculated for the 850–500-hPa layer and used as the parameterization of vertical velocity rather than $|\mathrm{VFI}|$ in (1). An empirical coefficient was determined via linear regression against the Summit accumulation data, as previously, and was applied to allow the quasigeostrophic (QG) ω-based model to yield realistic precipitation values. Although aware of the limitations of the use of (9) (e.g., mutual cancellation between the right-hand side terms) and the advantages of the **Q**-vector approach to calculating quasigeostrophic vertical motions (Trenberth 1978; Hoskins et al. 1978), we employed the more traditional approach for several reasons: (i) the **Q**-vector approach requires one more derivative and therefore a larger computational domain than (9), and we wanted to preserve as much horizontal spatial resolution as possible; and (ii) to answer the question of the role of baroclinicity, we needed some indication of the specific role of thermal advection, more easily gained through the use of (9) than through **Q** vectors.

The precipitation simulated by using the QG ω-based dynamic component was compared with that simulated by the VFI-based component. On a daily basis the results disagreed with regard to the placement of the precipitation maximum, but this is to be expected for two reasons: (i) there is an inherent phase difference of

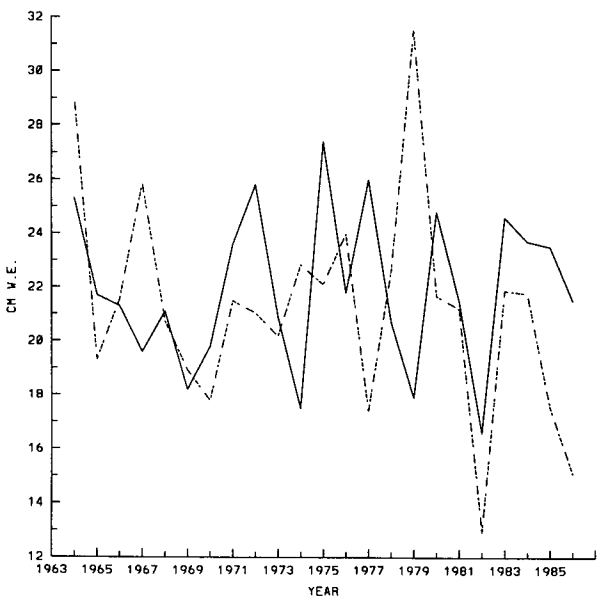

FIG. 4. Modeled annual dynamic precipitation for Summit (dashed) versus the observed accumulation time series (solid) used for fitting.

one-fourth wavelength between the flux of a quantity (as in VFI) and the advection of the same quantity [as in the vorticity advection term of (9)], and (ii) there is no representation of thermal advection in the VFI-based method. When the comparison is made between the two precipitation simulations summed over longer time periods (e.g., 1 year), however, much better agreement is found. Both methods produce the south-to-north decrease in precipitation. The QG ω-based method, however, produces smaller values and a much weaker spatial gradient of precipitation over southern and eastern Greenland than the VFI-based method. This is due to the increased area over which the QG calculations must be made with the resulting increased spatial smoothing of the calculated quantities. The general agreement over longer time periods between the two methods, which had disagreed on a daily basis, is due to (i) the effects of the aforementioned phase difference being minimized over longer time periods as modeled precipitation is accumulated due to successive storms tracking through the region, and (ii) the time mean pattern of the thickness advection term of (9) looking very similar to the time mean |VFI| for the Greenland area. Also, as will be discussed later, the trends in time found with the VFI-based dynamic component were also simulated with the QG ω-based method (see Fig. 10, which is introduced later). Therefore, as the VFI-based method provides essentially the same (and perhaps superior) results compared to the QG ω-based method for the time scales, which are the concern of this climatic study, it is preferred for several reasons. It is computationally much simpler, both in terms of data requirements and computational procedure. Only 500-hPa geopotential height data are required. This gives the method a wider range of applicability, perhaps even to global climate model (GCM) output, where 500-hPa geopotential height fields are often much better simulated than the precipitation fields (e.g., Tzeng et al. 1993). Fewer derivatives are involved in the VFI calculations, which allow for better spatial resolution in the results. Thus, for use as a climatic parameterization of precipitation, use of VFI is preferred over the more explicit QG ω.

c. *Orographic component*

As can be seen in Fig. 2, the steep coastal terrain gradients of Greenland present formidable obstacles to the flow of air. The importance of upslope precipitation over very long time periods was explored by Sanberg and Oerlemans (1983). In the present study, the vertical velocity due to the uplift of air over the terrain is taken to be directly proportional to

$$\mathbf{V}_{850} \cdot \nabla H \qquad (10)$$

(Haltiner 1971), where $\mathbf{V}_{850}$ is computed geostrophically from the 850-hPa NMC analyses, and H is the terrain height of Greenland. The 850-hPa level was chosen to ensure a strong effect of the topography on the airflow, as most of the ice sheet lies above the 850-hPa level. This orographic component is taken to be somewhat independent of the dynamic component due to the much smaller scale at which the terrain leads to uplift compared to the synoptic-scale forcing (Alpert and Shafir 1991). This is reflected in the fact that $\mathbf{V}_{850}$ is calculated on a roughly 400-km grid and then interpolated to the roughly 20-km grid of the terrain heights to make calculation of the orographic component possible. [The dynamic component is also linearly interpolated to this finer-scale grid to enable its addition to the orographic component in (1).] It should also be mentioned that this aspect of the model does not capture the effects of low-level blocking on the generation of near-coastal precipitation (Bromwich 1988).

As in the dynamic component, (10) is multiplied by q_{700} to capture the climatic seasonal cycle of the moisture content of the lower troposphere. The orographic component is only considered for cases where (10) is positive, that is, uplift. Thus, no downslope inhibition of precipitation or "snow-shadow" effects are considered.

Finally, an empirical coefficient A_1 is applied to allow this component to yield realistic precipitation values. Unlike the case for the dynamic component, however, no adequate glaciological data were found for the coastal slopes of the ice sheet with which to determine the value of this coefficient. Precipitation data from the ice-free coastal margins are available but are unreliable due to the problems associated with gauge measurements of snowfall (Woo et al. 1983), and even so would not capture the process under consideration here (i.e., precipitation over the coastal ice slopes). Thus, A_1 was chosen by an iterative trial and error procedure so as to provide the best subjective fit between the annual mean total precipitation for the 1963–89 period and maps of average annual accumulation and precipitation, such as those of Bender (1984; see his Fig. 6), Ohmura and Reeh (1991), and Radok et al. (1982). This procedure yielded $A_1 = 1500$ cm w.e. m^{-1} s.

The orographic component used here is an improvement over that presented in Keen (1984), which was based on VFI $\cdot \nabla H$. Thus, the effect of the topography on the 500-hPa geostrophic wind direction was captured, but at this level the contribution to vertical motion from orographic enhancement is likely to be small. The orographic component in Keen (1984) also led to unsatisfactory results, with an unrealistic decrease of precipitation via downslope flow over much of the eastern half of the ice sheet (S. A. Bowling 1990, personal communication).

3. Results

a. *Mean spatial patterns*

Figure 5 shows the computed mean annual precipitation for all of Greenland, expressed in cm w.e. For

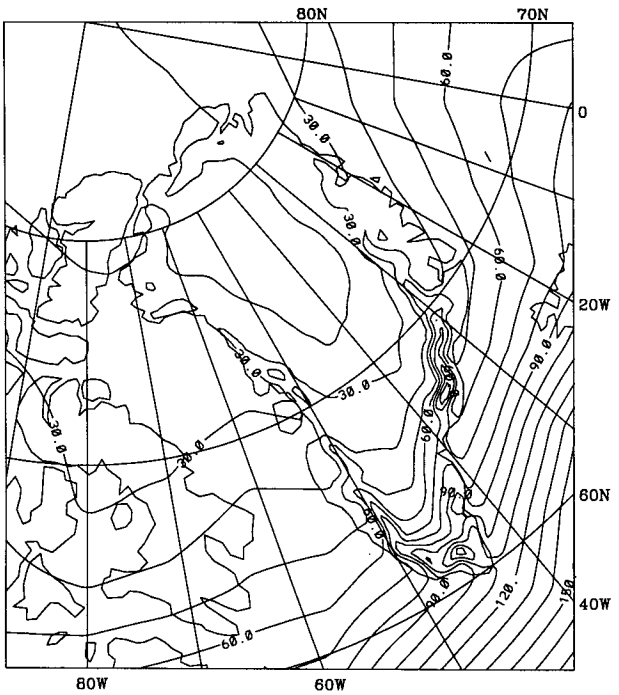

FIG. 5. Computed annual precipitation distribution for Greenland for 1963–89. The contour interval is 10 cm w.e.

comparison, the distribution of average annual accumulation in cm w.e. adapted from Bender (1984) is presented in Fig. 6. This depiction was derived from a synthesis of existing observed accumulation analyses, along with results from a simple model of orographic precipitation used to give the locations of the accumulation maximum along the coastal margins. [For a "purely" observational diagnosis of accumulation over Greenland, the reader is referred to Ohmura and Reeh (1991).]

The model is seen to successfully reproduce the most basic characteristics of the observed accumulation distribution. The general pattern of high values in the south to low values in the north is seen in the model results, as well as the zones of high accumulation along the southern coastal margins. The large area of low accumulation that dominates the northern interior is also simulated. There are important discrepancies, however, between the model results and the observed distribution. The modeled belt of high precipitation along the southeast coast appears too discontinuous. Low precipitation zones are lacking in the model results over the southern ice sheet "dome" in elevation and inland from Sondre Stromfjord. There is no modeled area of very low values (<10 cm w.e.) over the northern interior. Perhaps the model's most striking deficiency in simulating mean annual precipitation is its failure to simulate with sufficient magnitude or location the zone of high accumulation that runs inland along the northwestern coast from Jakobshavn to Thule. Possible explanations for this shortcoming are explored in section 4b.

The mean annual distribution of precipitation resulting from the dynamic and orographic components are separately shown in Figs. 7 and 8. It is clear that in this model the dynamic component is the dominant one, with the contribution of the orographic component limited to the coastal slopes, where the terrain height gradients are largest.

b. Temporal variability

1) INTERANNUAL

Figure 9 shows the time series of modeled total annual precipitation over the entire ice sheet for the period 1963–88. Superimposed on this is the best-fit linear trend. There is a clear downward trend in the modeled precipitation, with two fairly distinct time periods in evidence: a "wet" one from 1963 to 1973 and a "dry" one from 1974 to 1988 (with embedded years of high precipitation in 1983–84). A secondary trend upward during the dry period from 1977 to 1988 is also seen.

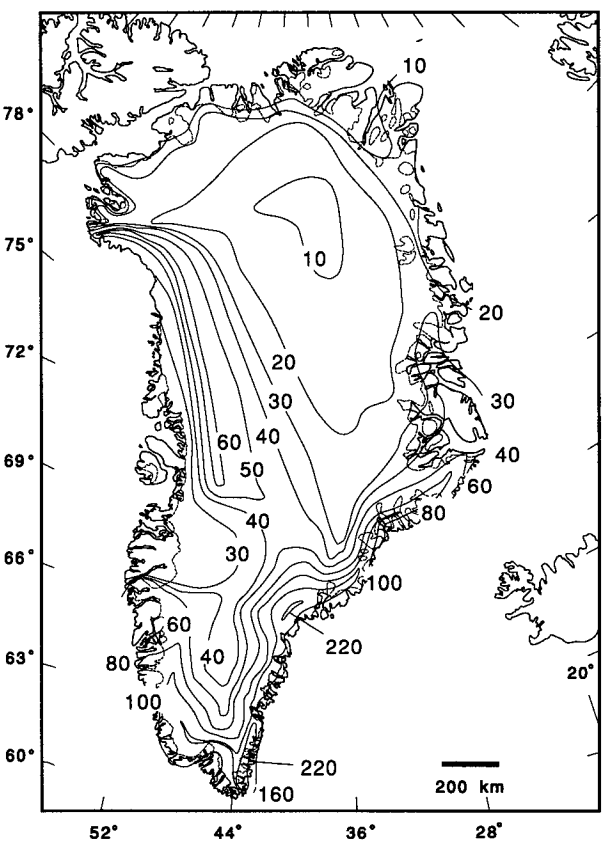

FIG. 6. Observed annual accumulation distribution over the Greenland Ice Sheet in centimeters water equivalent adapted from Bender (1984). The contour interval is 10 cm w.e. for values from 10 to 40; for values greater than 40 contours are provided for 50 (in northwest Greenland only), 60, 80, 100, 160, and 220 cm w.e.

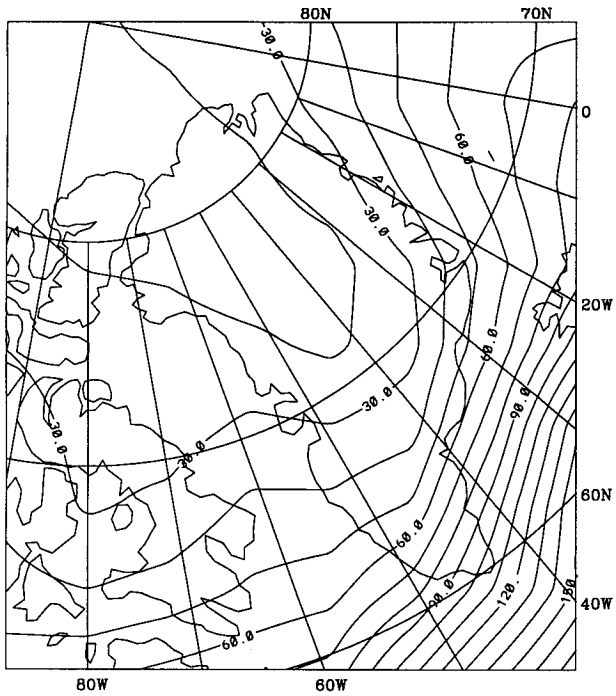

FIG. 7. Same as Fig. 5 but for the dynamic precipitation component.

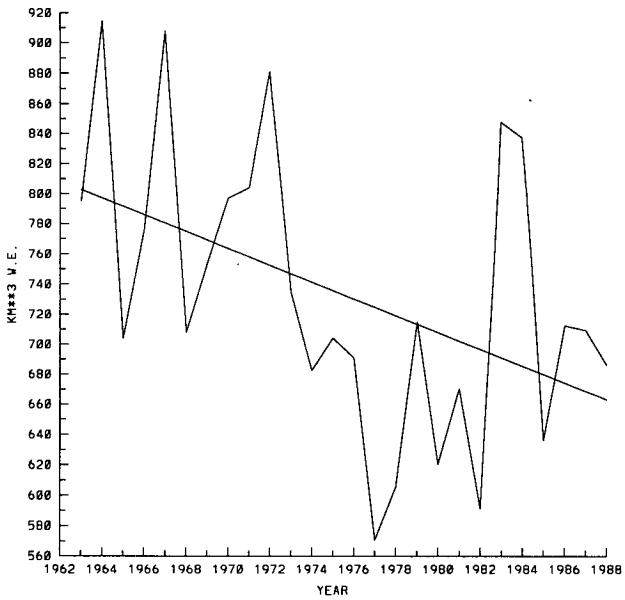

FIG. 9. Modeled total annual precipitation over the Greenland Ice Sheet for 1963–88 with linear regression trend [$y = (-5.6 \pm 2.3)x + (808.4 \pm 34.8)$, $r = 0.45$].

It is of interest to note that Zwally et al. (1989) have reported an elevation increase for the ice sheet south of 72°N using satellite radar altimetry data gathered from 1978 to 1986. Also note the high degree of year-to-year variability, with changes of 10% and more from one year to the next being fairly common. There appears to be about a 5-yr periodicity in the modeled precipitation series, as there was in the observational data collected at Summit (see Fig. 4).

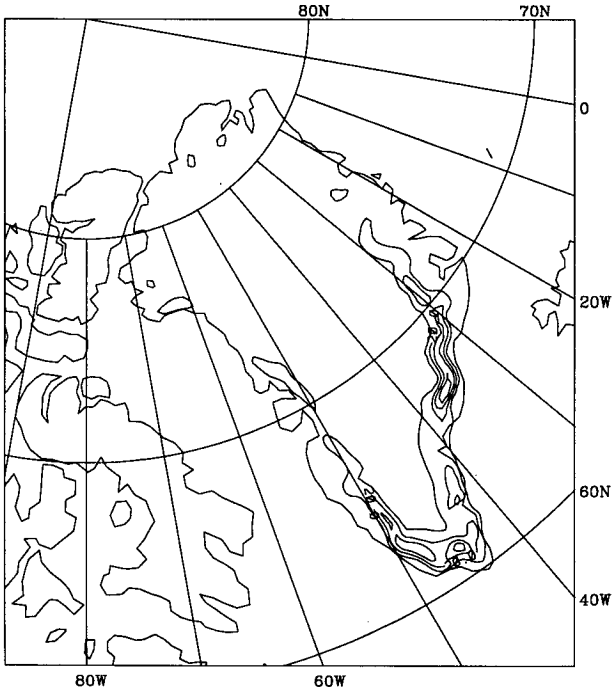

FIG. 8. Same as Fig. 5 but for the orographic precipitation component.

This trend in time toward smaller annual modeled precipitation was also simulated using the QG ω approach for the dynamic component, as was described in section 2b(3). This is shown in Fig. 10. [The smaller magnitudes in Fig. 10 as compared to Fig. 9 are due to (i) the previously mentioned smoothing involved in the use of the QG ω equation that substantially reduces the high precipitation values in southern Greenland and (ii) the lack of the orographic model component.] Linear regression between the time series of yearly precipitation over the entire ice sheet from the dynamic model component (which is very similar to Fig. 9) and Fig. 10 revealed that 64% of the variability in the QG ω-based time series is explained by the VFI-based time series. (The lack of complete agreement between the interannual variations in modeled precipitation from the two methods may also be due to the greater smoothing in the QG ω-based calculations. For example, areas of higher precipitation in the QG ω-based model may be smoothed out of Greenland in some years but not in others.) Thus, this time trend in the modeled precipitation is robust and not an artifact of the methods used to compute the VFI.

To investigate the spatial variations of the interannual variability, yearly model precipitation for 1963–88 (and the accompanying trend in time) is plotted in Fig. 11 for two different points on the ice sheet (see Fig. 1). Point *A* is meant to be a representative southern

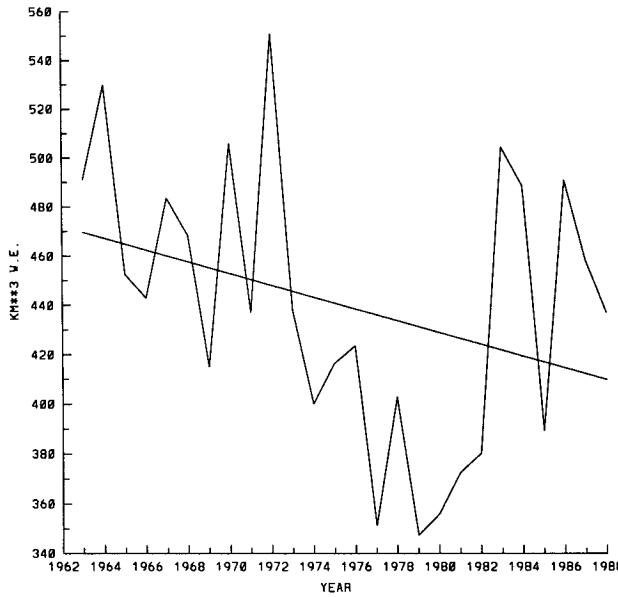

FIG. 10. As in Fig. 9 but from the dynamic component of the precipitation model based on QG $\omega[y = (-2.4 \pm 1.4)x + (472.0 \pm 21.8), r = 0.33]$.

coastal slope location, while point *B* is a point typical of the northern interior. The previously mentioned downward trend in time, as well as the large degree of year-to-year variability, is in evidence at both points (although only the linear trend for point *B* is statistically significant). The secondary upward trend during the latter half of the time period is seen for point *A*, but not for point *B*. Maps of mean annual precipitation from the model for representative periods of both generally high (1964–70) and low (1976–82) amounts are shown in Figs. 12 and 13. The patterns are similar in both cases. The higher values in Fig. 12 are increasingly larger than those in Fig. 13 from north to south.

2) INTRA-ANNUAL

Figure 14 shows the mean monthly model precipitation over the 1963–89 period for points *A* and *B*. Point *A* demonstrates fairly uniform precipitation from summer through early fall, then a precipitation maximum in October. The maximum precipitation at point *B* is modeled as occurring in August. This is in very close agreement with the seasonal variations in precipitation over Greenland summarized by Barry and Kiladis (1982). They reported a general fall maximum along the southeast coast south of 69°N, and a June–September maximum in the northern interior. They described marked spatial differences in the occurrence of the yearly precipitation maximum. Figure 15 shows the mean monthly precipitation over the entire ice sheet. There is a clear maximum in July and August. This is likely due to the direct dependence that the modeled precipitation has on specific humidity, with q_{700} having the climatologically largest values in late summer and early autumn. This dependence of modeled precipitation on specific humidity is enough to

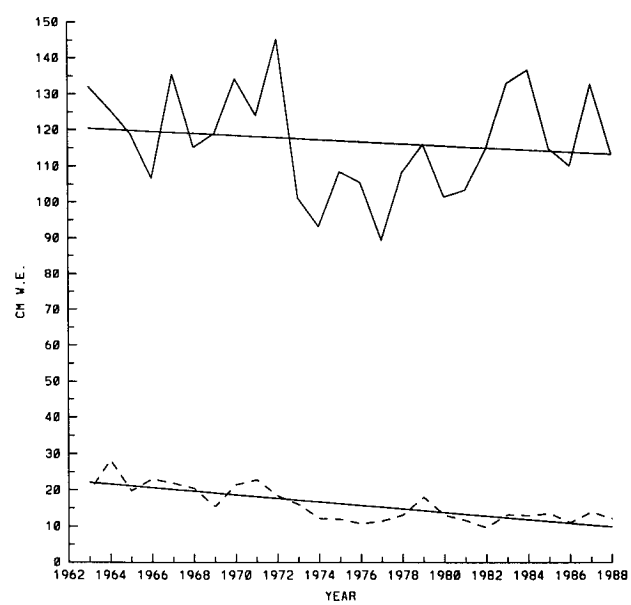

FIG. 11. Modeled precipitation time series at points A (solid) and B (dashed) together with linear regression trends; see Fig. 1 for locations.

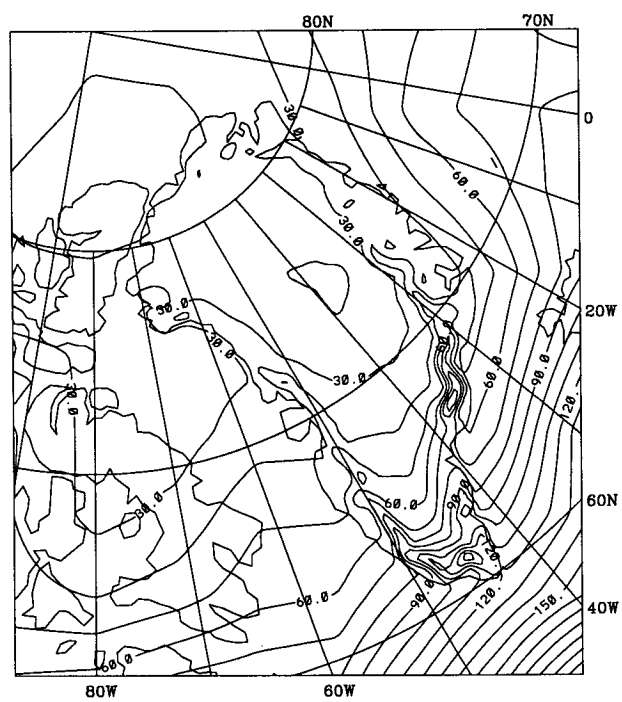

FIG. 12. Modeled spatial distribution of annual precipitation for the generally high precipitation period of 1964–70. The contour interval is 10 cm w.e.

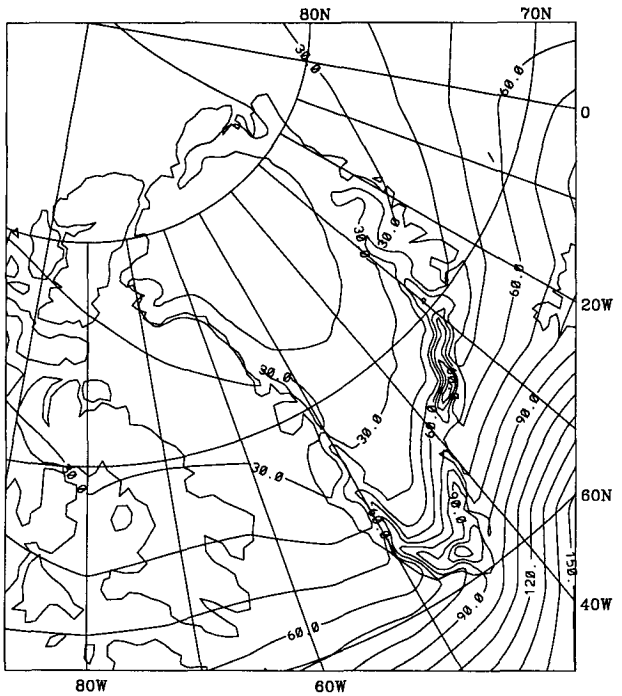

FIG. 13. Same as Fig. 12 but for the generally low precipitation period of 1976–82.

overwhelm the higher VFI, and therefore cyclonic activity, which is observed during winter and spring (not shown), a phenomenon that is also relevant in the actual meteorology of Greenland (Barry and Kiladis 1982).

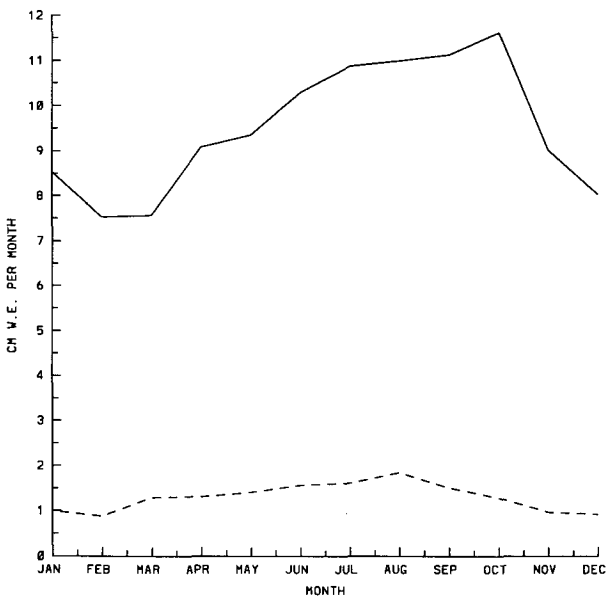

FIG. 14. Modeled intraannual variation of precipitation at points A (solid) and B (dashed); see Fig. 1 for locations.

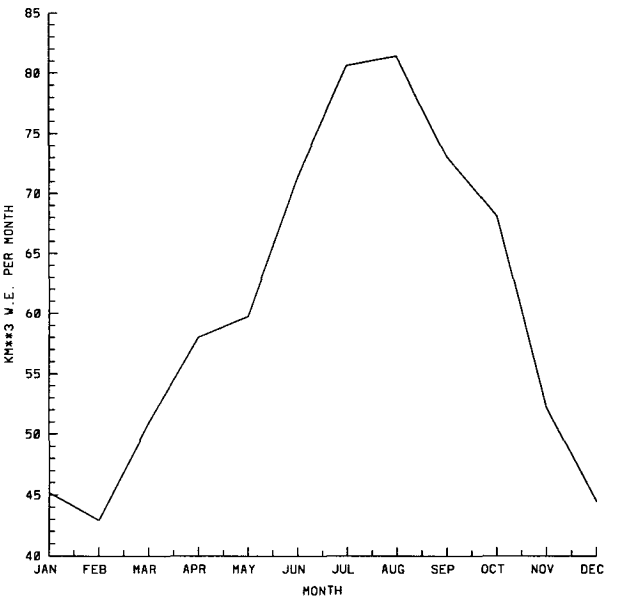

FIG. 15. Modeled intraannual variation in total precipitation summed over the Greenland Ice Sheet.

4. Discussion

a. Verification of results

As a check on the magnitudes of the simulated mean annual precipitation, the mean annual total precipitation over the entire ice sheet was computed, transformed into accumulation, and compared to other accumulation evaluations based on glaciological observations (Table 1). The model areal precipitation total was computed by finding all the grid points (on the fine scale) that lie over the ice sheet, multiplying their

TABLE 1. Mean annual accumulation estimates for the Greenland Ice Sheet (expanded from Bender 1984).

Source	Mean accumulation in kilometers cubed of water equivalent
Loewe (1936a,b)	355
Bauer (1955)	536
Bader (1961)	635
Benson (1962)	586
Loewe (1964)	588
Bauer (1967)	588
Radok et al. (1982)	675
Bender (1984)	716
Weidick (1984)	500 ± 100
Ohmura and Reeh (1991)	520
Current study	685*

* Based on a 7% difference between mean annual precipitation and accumulation (accumulation being the result of precipitation, net evaporation/sublimation, and drifting) found by Ohmura and Reeh (1991), the annual mean modeled accumulation is calculated from the 733 km^3 annual mean modeled precipitation over the ice sheet by dividing by 1.07.

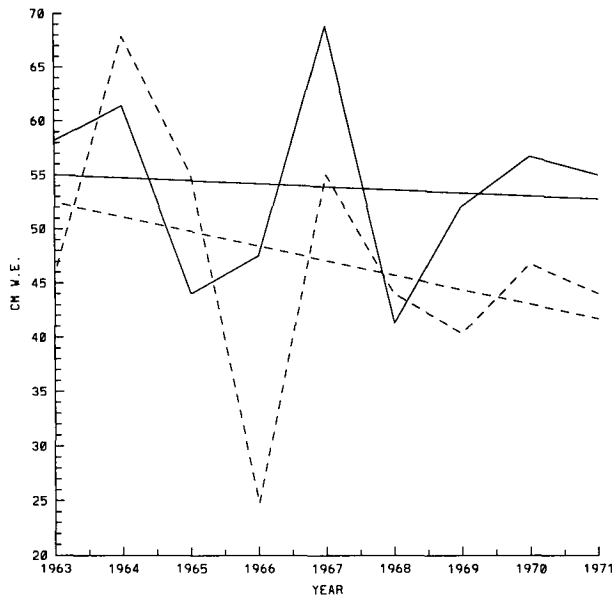

FIG. 16. Modeled annual precipitation (solid) for the Dye 3 area compared with observed annual accumulation (dashed, from Reeh et al. 1977), together with linear regression lines.

mean annual precipitation value by the area of the grid square centered on that point, and then summing all of these products. Examination of Table 1 shows that the model's value of total mean annual accumulation is close to the high end of the range of mean annual accumulations obtained by other investigators; however, the higher value obtained by Bender (1984) is preferred for comparison because he alone explicitly accounted for the large accumulation amounts over the coastal slopes. We conclude that the model is producing realistic time-averaged results.

As explained in section 2, the modeled dynamic precipitation amounts at Summit were fitted by regression analysis to the observed accumulation time series (see Fig. 4). Because the intercept of the regression line was set equal to zero, there is only one degree of freedom in the fit, and nothing requires the time trends of the two series to be equal. We found the slope of the regression line through the accumulation time series to be essentially zero, however, and the linear trend of the modeled precipitation time series to be slightly negative, but not statistically different from zero. Thus, the model appears to simulate the observed time trend of the accumulation at Summit.

Modeled trends in precipitation were also compared to accumulation time series from two other locations: Crete (Clausen et al. 1988) in central Greenland near Summit station, and Dye 3 (Reeh et al. 1977) in south-central Greenland (see Fig. 1). Both studies found annual accumulation rates to be decreasing for times overlapping with the period under consideration in this study (i.e., 1963–89). The 21-yr (1963–83) subset of the highly smoothed accumulation time series from the Crete area shows a decrease in yearly accumulation of 3% over these years, while the linear trend in the annual model precipitation for this area decreases by 13% over the same period (not shown). In Fig. 16 the model precipitation is compared directly to a 9-yr (1963–71) portion of the accumulation record at Dye 3. The trend in time is negative but not statistically significant for both time series. More remarkable is the similarity of the interannual variations. Thus, the model produces trends in annual precipitation that are qualitatively consistent with observed accumulation trends for two additional sites; it is remarkable that the very spatially smoothed dynamic precipitation amounts exhibit such consistency with "point" accumulation data for these locations.

Changes in the large-scale flow responsible for the negative precipitation tendency with time were sought by bandpass filtering of the model's input 500-hPa data. A Lanczos filtering scheme (Duchon 1979) for 2–6-day variations was performed on the NMC data for both the 0000 and 1200 UTC analyses, for the contrasting time periods of 1964–70 (high precipitation) and 1976–82 (low precipitation). The average daily variability for each period is shown in Figs. 17 and 18. Both plots show a large area of high variability located over northeastern North America and extending into the North Atlantic. Comparison of these two figures reveals that for 1964–70 (Fig. 17) the magnitudes in this area are larger (i.e., more variability) and that its axis (the 500-hPa storm track) turns northward and passes just to the east of Iceland rather than continuing across the North Atlantic to Scandinavia (1976–1982,

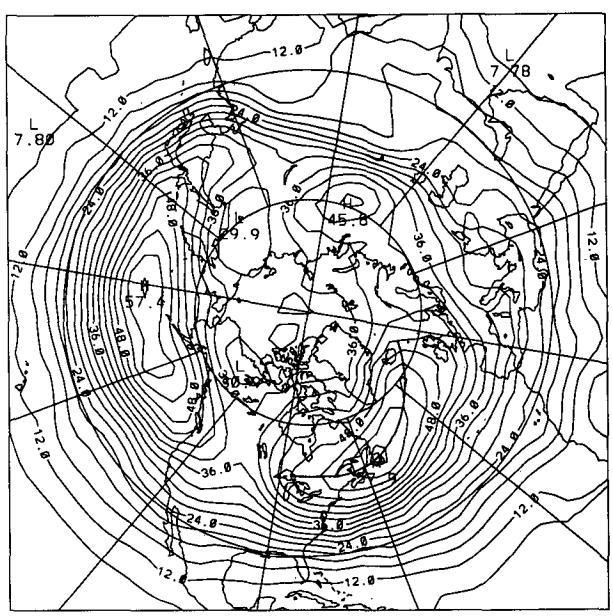

FIG. 17. Variability on the synoptic time scale (in geopotential meters) of the 500-hPa geopotential height field for the generally high precipitation period of 1964–70. The axis of maximum variability in the North Atlantic is also indicated.

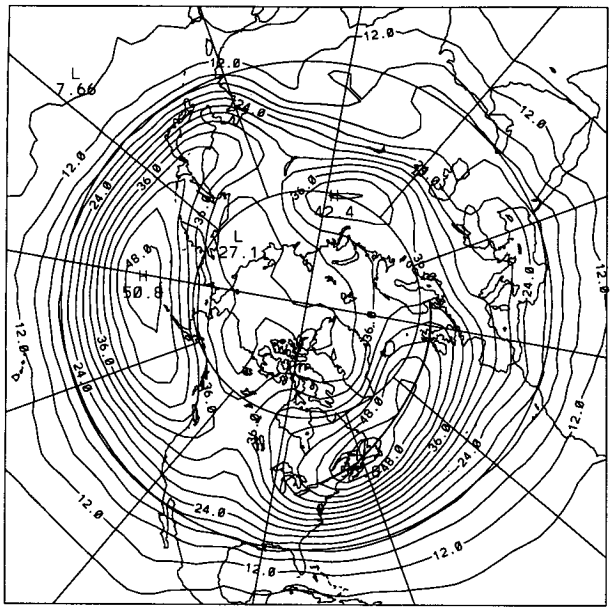

FIG. 18. Same as Fig. 17 but for the generally low precipitation period of 1976–82.

Fig. 18). Thus, there was more cyclonic activity near Greenland during 1964–70, with its axis of maximum variability located closer to Greenland, and a physically meaningful and consistent change in the storm track between these two periods is observed.

Climatological monthly mean values of specific humidity were used in this model. It is possible that a temporally increasing trend in the actual specific humidity values could counteract or even overwhelm the downward trend in modeled mean annual precipitation. It has already been noted how sensitive the modeled precipitation is to temporal variations of q_{700}. To explore this possibility, monthly mean values of specific humidity at the 700-hPa level for 1963–89 were computed from dewpoint temperatures given in *Monthly Climatic Data for the World* for the southern coastal radiosonde stations of Narssarssuaq and Angmagssalik (see Fig. 1 for locations). The annual mean values and their corresponding linear trends are shown in Fig. 19. Although there is a large interannual variability at both sites with extremes reaching ±20% of the mean, there is a weak downward trend. It appears that the simulated decrease in precipitation is not an artifact arising from use of climatological specific humidities.

Furthermore, comparison of Fig. 19 with the time series of precipitation over the entire ice sheet (Fig. 9) reveals a qualitative similarity in the interannual variabilities. This seems reasonable and physically meaningful as times of increased modeled precipitation (essentially, increased VFI) would also be times of increased upward vertical motion and convergence of lower tropospheric air, which would lead to a higher moisture content in the lower troposphere. Corresponding reasoning would apply for periods of decreased modeled precipitation. Once again physical consistency is evident, this time between two quantities that are computationally entirely independent.

This overall trend in time toward smaller precipitation rates is also consistent with the observed trend of less cyclones and cyclogenesis over North America and surrounding waters during the periods 1950–77 (Zishka and Smith 1980) and 1958–77 (Whittaker and Horn 1981). Many of these cyclones reach the Greenland area (Whittaker and Horn 1984). Both studies showed larger, more significant downward trends in cyclone frequency for January as compared with July. As a further check of the model, the time series of simulated precipitation for the whole of Greenland was decomposed into the four seasons (not shown). The trend toward smaller annual precipitation was much more evident in the winter season (December, January, February) than in summer (June, July, August). The largest downward trend in modeled precipitation, however, was seen to occur in autumn (September, October, November), which is not consistent with Whittaker and Horn (1981), who found October cyclogenesis decreasing at a smaller rate than that for July.

b. Influence of NMC analysis scheme(s)

Three major changes in NMC's analysis procedures occurred during the period for which 500-hPa data are available (1946–89; D. Joseph 1991, personal com-

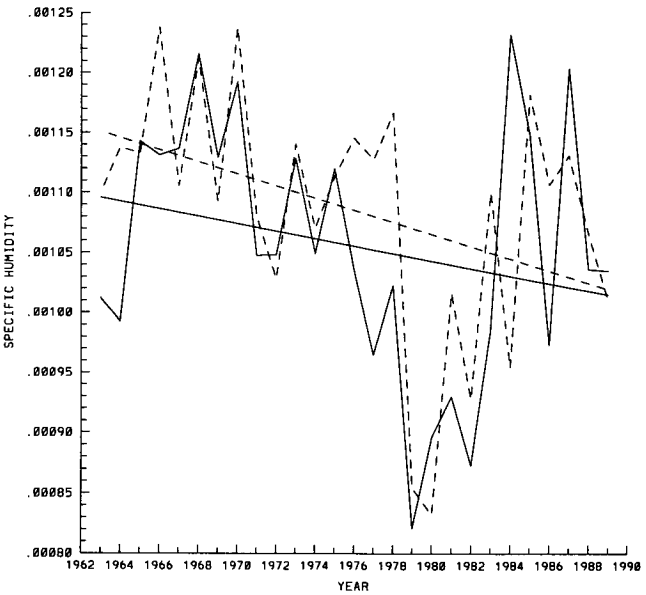

FIG. 19. Annual mean specific humidities at the 700-hPa level for Narssarssuaq (dashed) and Angmagssalik (solid) radiosonde stations with linear regression trends [Angmagssalik: $y = (-3.3 \times 10^{-6} \pm 2.8 \times 10^{-6})x + (1.1 \times 10^{-3} \pm 4.4 \times 10^{-5})$, $r = 0.23$; Narssarssuaq: $y = (-5.0 \times 10^{-6} \pm 2.6 \times 10^{-6})x + (1.2 \times 10^{-3} \pm 3.9 \times 10^{-5})$, $r = 0.37$].

munication). In December 1962 an objective analysis was implemented, replacing various hand analyses. A switch from Cressman to a spectral (Hough) analysis scheme was made in September 1974. An optimal interpolation scheme was implemented in September 1978. Of these changes, the one in 1962 is believed to be responsible for a major shift in the precipitation estimates produced by this model. Figure 20 shows the time series of modeled annual precipitation from the dynamic component at Summit for 1946–1988. Note the relatively abrupt increase that took place during 1960–1962. Although not all Summit ice cores extend back to this time, those that do show no evidence of this precipitation increase (Bolzan and Strobel 1993). Wahl (1972), in a derivation and study of 700-hPa meridional and zonal indices, also encountered abrupt and otherwise unexplainable changes in these indices in the early 1960s, which he attributed to this same analysis change at NMC. It was primarily to avoid this problem that the early part of the NMC 500-hPa data (1946–62) was not used in the present study. By contrast, the analysis changes of 1974 and 1978 produced no obvious sustained change in the simulated precipitation rate.

It is also conjectured that a shortcoming in the NMC analyses is responsible for the model's poor simulation of the belt of high accumulation along the northern west slopes of Greenland. It is likely that this high accumulation area arises from orographically forced uplift of air flowing from the west and southwest (Ohmura and Reeh 1991), such as would occur around the southern and eastern sides of cyclones that are known to develop, as well as move into, the Davis Strait/Baffin Bay region (Putnins 1970; Keen 1980; Barry and Kiladis 1982). An underrepresentation of the strength, or the frequency of these cyclones, or both would lead directly to an underestimation of the orographic precipitation along the western coast in the model. Figure 21 shows the mean daily variability on synoptic time scales from applying the previously mentioned bandpass filter to the twice-daily sea level pressure fields for 1963–89. Some evidence for a storm track just off the west coast of Greenland is observed in the lobe of higher variability that extends northward along the western coast of Greenland. Serreze and Barry (1988) also report an underestimation of Baffin Bay cyclones for all seasons in the NMC analyses.

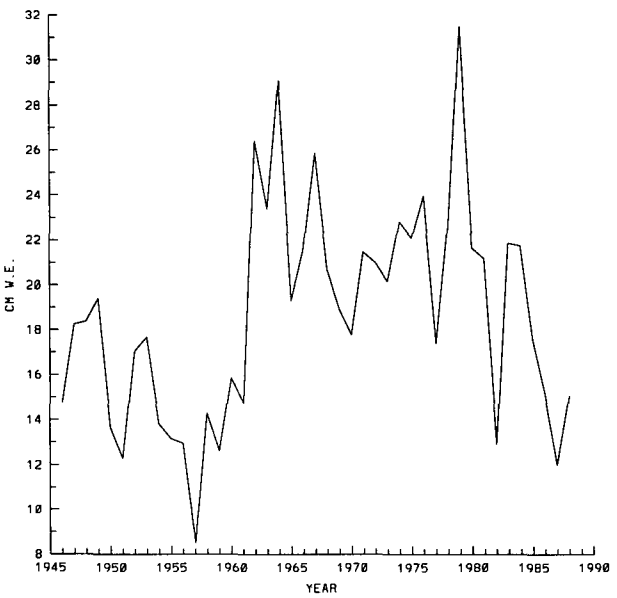

FIG. 20. Modeled dynamic precipitation at Summit for 1946–88 illustrating the anomalous jump around 1961/1962.

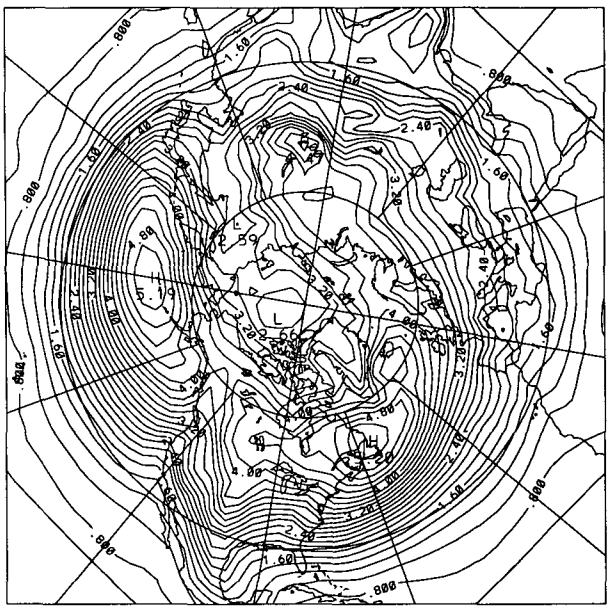

FIG. 21. Variability on the synoptic time scale of the sea level pressure field (in hPa) for 1963–89.

The question as to why the NMC analyses might underestimate the activity of the west coast storm track cannot be answered at present, but a plausible reason can be advanced. Mesoscale cyclones develop with great frequency around the coast of Antarctica in conjunction with katabatic winds from the ice sheet and are poorly represented in observational analyses for those areas because of their small size and general lack of distinctive satellite signatures (Bromwich 1991). These features apparently appear in present-day simulations produced by the NCAR Community Climate Model Version 1 (a general circulation model) and play an important role in simulated snowfall formation over the Antarctic ice sheets (Tzeng et al. 1993). It is suggested that such a mechanism may be active in conjunction with the katabatic airflow off the west side of the Greenland Ice Sheet, similar to what happens just off its southeastern coast (Mansfield 1974). Also, isolated small-scale "polar lows" are known to occur in

the Davis Strait/Baffin Bay region (Parker and Hudson 1991; Rasmussen and Purdom 1992); these often form over open water as cold air blows off eastern Canada during winter. Such unrepresented cyclonic activity (whether they were not analyzed by NMC or were absent due to the coarse resolution of the gridded datasets) may be the cause of the inability of our model to simulate the orographic snowfall maximum along the northwestern section of the ice sheet. These vortices should move northward following the usual storm track in this area. Substantial efforts will be needed to ascertain whether such developments, which probably result from a marked interaction between the synoptic- and mesoscales, occur with the frequency required to explain this modeled precipitation shortcoming.

c. Implications and extensions

The results have revealed a very large interannual variability in the water mass deposited onto the Greenland Ice Sheet by the atmosphere over the last two-and-a-half decades. There is a downward trend in the precipitation rate amounting to about 15% during 1963–88. The trend is associated with systematic changes in the location and intensity of the dominant storm track passing to the south and east of Greenland. The modeled precipitation trend is substantiated by independent records and is not counterbalanced by an increase in the average moisture content of the air. The latter does, however, exhibit large interannual variability, and the impact of using actual rather than climatological moisture values is being explored with an enhanced version of the model.

The results of this study are relevant to the question of global sea level change. Warrick and Oerlemans (1990), in a summary of sensitivity studies of Greenland Ice Sheet mass balance to various climatic parameters, report a fall of ~0.1 mm resulting from a 5% increase in precipitation over Greenland. (This is ignoring any corresponding changes in temperature, cloud cover, or other factors affecting mass balance.) Inferring a precipitation decrease of 15% during 1963–88 from the linear trend of yearly modeled precipitation over the ice sheet, a contribution of ~0.3 mm yr^{-1} to global sea level would have resulted by the end of this period, if the ice sheet was in balance in 1963. It is therefore possible that Greenland has contributed to recently observed increases in global sea level (Douglas 1991).

Other climatic changes in this region have been documented by Chapman and Walsh (1993). They report that southern Greenland and the adjacent waters of Baffin Bay, the Labrador Sea, and the North Atlantic have undergone a significant cooling in surface air temperatures during the period 1961–90, in contrast to warming during this same period observed over the rest of the Northern Hemisphere north of 50°N. This cooling in the Greenland region has a maximum of 0.6°C per decade and is manifested in all seasons, although most striking in autumn and winter (also the seasons in which the modeled trend toward less precipitation over Greenland is most marked, as mentioned previously). Chapman and Walsh (1993) also report increasing sea ice extents over Baffin Bay and the Labrador Sea during the last three decades, with decreasing sea ice extents to the east of Greenland between the longitudes of 40°W and 40°E. Similar changes in sea ice extent are also described in Mysak and Manak (1989). Clearly more work needs to be done to investigate the dynamic links involved, as well as in relating the interannual variability of the modeled precipitation to Northern Hemispheric climatic indicators such as the "North Atlantic oscillation" (van Loon and Rogers 1978).

Mention is often made in studies involving accumulation in the polar regions of the positive correlation between accumulation (or precipitation) and air temperature, due to the exponential dependence of the saturation vapor pressure of air on temperature. Zwally (1989) summarizes, from other investigations using a variety of approaches, a range of precipitation changes of from 5% to 20% per degree Celsius, while Morgan et al. (1991) cite a range from 3% to 10% per degree Celsius. In the current study, a positive correlation between temperature and precipitation is also seen, as Chapman and Walsh (1993) (in their Fig. 1) indicate a mean temperature decrease over the Greenland Ice Sheet of roughly 0.25°C per decade during 1961–90, and we find a modeled precipitation decrease of ~15% during 1963–88. It should be made clear, however, that the modeled precipitation changes cannot be explained by the temperature changes, as the modeled precipitation changes are larger (~25% per °C) than would be expected from the aforementioned relationships alone. Morgan et al. (1991) found the same to be true of their observed accumulation increases for 1960–85 over a portion of East Antarctica (~50% per °C). The precipitation trends result primarily from changes in the frequency and intensity of transitory precipitation events, and the relationship between these events and temperature changes are quite complex. Furthermore, changes in the precipitation events can themselves lead to temperature changes, so that both the temperature and precipitation trends may in large measure result from a common cause.

Superimposed on the downward precipitation trend is an ~5-yr periodicity that shows up in both the modeled time series and the observed accumulation amounts near Summit. This is reminiscent of the 5.5-yr periodicity of an index (normalized winter mean sea level pressure anomalies at Darwin) related to the Southern Oscillation (Rogers 1984); in fact, there are strong modeled precipitation peaks (see Fig. 9) near the strong El Niño events of 1972–73 and 1982–83. At other times, however, no such association is

manifested. For example, the El Niño event of 1976–77 corresponds to very low modeled precipitation over Greenland. This aspect of the modeled precipitation trend also requires more investigation.

Interannual precipitation variations of the magnitude found here are of importance to attempts to infer the spatial distribution of annual accumulation rate over the ice sheet (like Fig. 6) because normally no allowance is made in such analyses for the varying record durations and times at which the measurements were collected, that is, the analyses are not normalized to a fixed climatological period. From a broader perspective such variations impact evaluations of the mass budget of the ice sheet; at present, the uncertainties associated with the other terms in the mass budget, such as meltwater runoff, are much larger than those associated with the precipitation input (Reeh 1985). Finally, such variability should be taken into account in modeling the flow of glacier ice where the mass input from the atmosphere is an important upper-boundary condition that is usually treated in a simplistic manner (often taken to be constant in time).

With regard to the satellite radar altimetry results mentioned several times, it is interesting to note from Fig. 11 that the 7-yr period over which Zwally et al. (1989) found ice sheet elevation increases (1978–86) coincides with a trend toward greater values in modeled precipitation over the Greenland Ice Sheet south of 72°N (not shown). This modeled trend amounts to a 15% increase in precipitation during 1978–86, which translates to an areally averaged value of 7 cm w.e. Assuming a low density for fallen and compressed snow of 460 kg m^{-3} compared with an ice density of 920 kg m^{-3} (Van der Veen 1993), this could account, considered in isolation, for a surface rise of about 0.15 m, or only about 9% of the elevation increase found by Zwally et al. (1989). The extremely high precipitation values calculated for 1983 and 1984 strengthens the contention that part of the altimeter-observed thickening may be due to recent precipitation increases.

Acknowledgments. This work was primarily sponsored by the National Oceanic and Atmospheric Administration's Climate and Global Change Program through Grant NA90 AA-D-AC504 to D. H. Bromwich. J. F. Bolzan's contribution was supported by National Science Foundation Grants DPP-8520855 and DPP-8822081. We thank H. Jay Zwally for helpful comments on the implications of our results, especially relating to the question of global sea level rise. We also thank an anonymous reviewer for comments concerning the theoretical basis of the precipitation model. C. Benson kindly provided a high quality version of what we adapted to become Fig. 6. R.-Y. Tzeng carried out the Lanczos filtering calculations presented in Figs. 17, 18, and 21. Kathy Doddroe and Linda Buchan typed the original manuscript.

REFERENCES

Alpert, P., and H. Shafir, 1991: Role of detailed wind-topography interaction in orographic rainfall. *Quart. J. Roy. Meteor. Soc.*, **117,** 421–426.

Bader, H., 1961: The Greenland Ice Sheet, CRREL Monograph I-B2, U.S. Army Cold Regions Research and Engineering Laboratory, Hanover, New Hampshire, 18 pp.

Barry, R. G., and G. N. Kiladis, 1982: Climatic characteristics of Greenland. *Climatic and Physical Characteristics of the Greenland Ice Sheet,* U. Radok, R. G., Barry, D. Jenssen, R. A. Keen, G. N. Kiladis, B. McInnes, Eds. CIRES, Univ. Colorado, 7–33.

Bauer, A., 1955: The balance of the Greenland Ice Sheet. *J. Glaciol.,* **2**(17), 456–462.

——, 1967: Nouvelle estimation du bilan de masse de l'Inlandsis du Groenland. *Deep-Sea Res.,* **14,** 13–17.

Bender, G., 1984: The distribution of snow accumulation on the Greenland Ice Sheet. M.S. thesis, Geophysical Institute, University of Alaska, Fairbanks, Alaska, 110 pp.

Benson, C. S., 1962: *Stratigraphic Studies in the Snow and Firn of the Greenland Ice Sheet.* CRREL Research Report 70, U.S. Army Cold Regions Research and Engineering Laboratory, Hanover, New Hampshire, 93 pp.

Blackmon, M. L., R. A. Madden, J. M. Wallace, and D. S. Gutzler, 1979: Geographical variations in the vertical structure of geopotential height fluctuations. *J. Atmos. Sci.,* **36,** 2450–2466.

Bolzan, J. F., and M. Strobel, 1993: Accumulation rate variations around Summit, Greenland. *J. Glaciol.,* in press.

Bromwich, D. H., 1988: Snowfall in high southern latitudes. *Rev. Geophys.,* **26,** 149–168.

——, 1991: Mesoscale cyclogenesis over the southwestern Ross Sea linked to strong katabatic winds. *Mon. Wea. Rev.,* **119,** 1736–1752.

Chapman, W. L., and J. E. Walsh, 1993: Recent variations of sea ice and air temperatures in high latitudes. *Bull. Amer. Meteor. Soc.,* **74,** 33–47.

Charney, J. G., 1949: On a physical basis for numerical prediction of large-scale motions in the atmosphere. *J. Meteorol.,* **6,** 371–385.

Clausen, H. B., N. S. Gundestrup, S. J. Johnsen, R. Bindschadler, and H. J. Zwally, 1988: Glaciological investigations in the Crete area, central Greenland: A search for a new deep-drilling site. *Annals Glaciol.,* **10,** 10–15.

Commission for Scientific Research in Greenland, 1989: Ice core drilling. *Newsletter,* No. 18, 48–50.

Crutcher, H. L., and J. M. Meserve, 1970: Selected Level Heights, Temperatures, and Dew Points for the Northern Hemisphere. NAVAIR Report 50-1C-52, U.S. Government Printing Office, Washington, D.C., 426 pp.

Douglas, B. C., 1991: Global sea level rise. *J. Geophys. Res.,* **96,** 6981–6992.

Douglas, B. C., R. E. Cheney, L. Miller, R. W. Agreen, W. E. Carter, and D. S. Robertson, 1990: Greenland Ice Sheet: Is it growing or shrinking? *Science,* **248,** 288.

Duchon, C. E., 1979: Lanczos filtering in one and two dimensions. *J. Appl. Meteor.,* **18,** 1016–1022.

Fjortoft, R., 1952: On a numerical method of integrating the barotropic vorticity equation. *Tellus,* **4,** 179–194.

Godske, C., T. Bergeron, J. Bjerknes, and R. Bundgaard, 1957: *Dynamic Meteorology and Weather Forecasting.* Amer. Meteor. Soc., 808 pp.

Haltiner, G. J., 1971: *Numerical Weather Prediction.* John Wiley, 317 pp.

Holton, J. R., 1992: *An Introduction to Dynamic Meteorology,* third ed. Chapter 6, Academic Press, 166–170.

Hoskins, B. J., I. Draghici, and H. C. Davies, 1978: A new look at the ω-equation. *Quart. J. Roy. Meteor. Soc.,* **104,** 31–38.

Jenne, R., 1970: *The NMC Octagonal Grid.* National Center for Atmospheric Research, 13 pp.

Johnsen, S. J., H. B. Clausen, W. Dansgaard, K. Fuhrer, N. Gun-

destrup, C. U. Hammer, P. Iversen, J. Jouzel, B. Stauffer, and J. P. Steffensen, 1992: Irregular glacial interstadials recorded in a new Greenland ice core. *Nature,* **359,** 311–313.

Johnsen, S. J., W. Dansgaard, and J. W. C. White, 1989: The origin of Arctic precipitation under present and glacial conditions. *Tellus,* **41B,** 452–468.

Keen, R. A., 1980: *Temperature and Circulation Anomalies in the Eastern Canadian Arctic Summer 1946–76.* Occasional Paper 34, Institute of Arctic and Alpine Research, Univ. of Colorado, Boulder, Colorado, 159 pp.

——, 1984: Statistical-dynamical model of accumulation on the Greenland Ice Sheet. *Annals Glaciol.,* **5,** 69–74.

Kelly, P. M., P. D. Jones, C. B. Sear, B. S. G. Cherry, and R. K. Tavakol, 1982: Variations in surface air temperatures: Part 2. Arctic regions, 1881–1980. *Mon. Wea. Rev.,* **110,** 71–83.

Kostecka, J. M., and I. M. Whillans, 1988: Mass balance along two transects of the west side of the Greenland Ice Sheet. *J. Glaciol.,* **34,** 31–39.

Langway, C. C., H. Oeschger, and W. Dansgaard, Eds., 1985: *Greenland Ice Core: Geophysics, Geochemistry and the Environment.* Geophysical Monograph 33, Amer. Geophys. Union, 118 pp.

Lau, N.-C., 1979: The structure and energetics of transient disturbances in the Northern Hemisphere wintertime circulation. *J. Atmos. Sci.,* **36,** 982–995.

Loewe, F., 1936a: Höhenverhältnisse und Massenhaushalt des grönländischen Inlandeises. *Gerlands Beitr. zur Geophys.,* **46,** 317–330.

——, 1936b: Höhenverhältnisse und Massenhaushalt des grönländischen Inlandeises. Nachträge und Berichtigung, *Gerlands Beitr. zur Geophys.,* **48,** 86–89.

——, 1964: Das grönländische Inlandeis nach neuen Feststellungen. *Erdkunde,* **18**(3), 189–202.

Mansfield, D. A., 1974: Polar lows: The development of baroclinic disturbances in cold air outbreaks. *Quart. J. Roy. Meteor. Soc.,* **100,** 541–554.

Morgan, V. I., I. D. Goodwin, D. M. Etheridge, and C. W. Wookey, 1991: Evidence from Antarctic ice cores for recent increases in snow accumulation. *Nature,* **354,** 58–60.

Mysak, L. A., and D. K. Manak, 1989: Arctic sea-ice extent and anomalies, 1953–1984. *Atmos.-Ocean,* **27,** 376–405.

Ohmura, A., 1987: New temperature distribution maps for Greenland. *Zeit. Gletsch. Glazial.,* **23,** 1–45.

——, and N. Reeh, 1991: New precipitation and accumulation maps for Greenland. *J. Glaciol.,* **37,** 140–148.

Palmén, E., and C. W. Newton, 1969: *Atmospheric Circulation Systems.* Academic Press, 603 pp.

Parker, N., and E. Hudson, 1991: *Polar Low Handbook for Canadian Meteorologists.* Atmospheric Science Service, Environment Canada, 173 pp.

Peltier, W. R., and A. M. Tushingham, 1989: Global sea level rise and the Greenhouse effect: Might they be connected? *Science,* **244,** 806–810.

Putnins, P., 1970: The climate of Greenland. *Climates of the Polar Regions,* S. Orvig, Ed. World Survey of Climatology, Vol. 14, Elsevier, 3–128.

Radok, U., R. G. Barry, D. Jenssen, R. A. Keen, G. N. Kiladis, and B. McInnes, 1982: *Climatic and Physical Characteristics of the Greenland Ice Sheet.* CIRES, Univ. of Colorado, Boulder, Colorado, 193 pp.

Rasmussen, E. A., and J. F. W. Purdom, 1992: Investigations of a polar low using geostationary satellite data. *Sixth Conference on Satellite Meteorology and Oceanography, Preprint Volume,* Atlanta, Georgia, Amer. Meteor. Soc., 120–122.

Rasmussen, L., 1989: Greenland winds and satellite imagery. *Vejret,* Danish Meteor. Soc., 32–37.

Reeh, N., 1985: Greenland ice-sheet mass balance and sea-level change. *Glaciers, Ice Sheets and Sea Level: Effect of a CO_2-Induced Climatic Change,* Publ. DOE/ER/60235-1, Dept. of Energy, Washington, D.C., 155–171.

——, H. B. Clausen, N. Gundestrup, S. J. Johnsen, and B. Stauffer, 1977: $\delta(^{18}O)$ and accumulation rate distribution in the Dye 3 area, south Greenland. International Association for Hydrological Sciences, Pub. No. 118, 177–181.

Rogers, J. C., 1984: The association between the North Atlantic oscillation and the Southern Oscillation in the Northern Hemisphere. *Mon. Wea. Rev.,* **112,** 1999–2015.

——, and H. van Loon, 1979: The seesaw in winter temperatures between Greenland and northern Europe. Part II: Some atmospheric and oceanic effects in middle and high latitudes. *Mon. Wea. Rev.,* **107,** 509–519.

Sanberg, J. A. M., and J. Oerlemans, 1983: Modelling of Pleistocene European ice sheets: The effect of upslope precipitation. *Geol. Mijnbouw,* **62,** 267–273.

Scorer, R. S., 1988: Sunny Greenland. *Quart. J. Roy. Meteor. Soc.,* **114,** 3–29.

Serreze, M. C., and R. G. Barry, 1988: Synoptic activity in the Arctic Basin, 1979–85. *J. Climate,* **1,** 1276–1295.

Stearns, C. R., and G. A. Weidner, 1991: The polar automatic weather station project of the University of Wisconsin. *Proc. of the International Conference on the Role of the Polar Regions in Global Change, Vol. I,* G. Weller, C. L. Wilson, and B. A. B. Severin, Eds., University of Alaska Fairbanks, Fairbanks, Alaska, 58–62.

Trenberth, K., 1978: On the interpretation of the diagnostic quasi-geostrophic omega equation. *Mon. Wea. Rev.,* **106,** 131–137.

Tzeng, R.-Y., D. H. Bromwich, and T. R. Parish, 1993: Present-day Antarctic climatology of the NCAR Community Climate Model Version 1. *J. Climate,* **6,** 205–226.

Van der Veen, C. J., 1993: Interpretation of short-term ice-sheet elevation changes inferred from satellite altimetry. *Climatic Change,* in press.

van Loon, H., and J. C. Rogers, 1978: The seesaw in winter temperatures between Greenland and northern Europe. Part I: General description. *Mon. Wea. Rev.,* **106,** 296–310.

Wahl, E., 1972: Climatological studies of the large-scale circulation in the Northern Hemisphere: 1. Zonal and meridional indices at the 700-millibar level. *Mon. Wea. Rev.,* **100,** 553–564.

Warrick, R. A., and J. R. Oerlemans, 1990: Sea level rise. *Climate Change: The IPCC Scientific Assessment,* J. T. Houghton, G. J. Jenkins, and J. J. Ephraums, Eds., Cambridge University Press, 257–281.

Weidick, A., 1984: Studies of glacier behaviour and glacier mass balance in Greenland—A review. *Geogr. Ann.,* **66A**(3), 183–195.

Weidner, G. A., and C. R. Stearns, 1991: A two-year record of the climate on the Greenland crest from an automatic weather station. *Proc. of the International Conference on the Role of the Polar Regions in Global Change, Vol. I,* G. Weller, C. L. Wilson, and B. A. B. Severin, Eds., University of Alaska Fairbanks, Fairbanks, Alaska, 220–222.

Whittaker, L. M., and L. H. Horn, 1981: Geographical and seasonal distribution of North American cyclogenesis, 1958–1977. *Mon. Wea. Rev.,* **109,** 2312–2322.

——, and ——, 1984: Northern Hemisphere extratropical cyclone activity for four mid-season months. *J. Climatol.,* **4,** 297–310.

Woo, M.-K., R. Heron, P. Marsh, and P. Steer, 1983: Comparison of weather station snowfall with winter snow accumulation in high Arctic basins. *Atmos.-Ocean,* **21,** 312–325.

Zishka, K. M., and P. J. Smith, 1980: The climatology of cyclones and anticyclones over North America and surrounding ocean environs for January and July, 1950–77. *Mon. Wea. Rev.,* **108,** 387–401.

Zwally, H. J., 1989: Growth of Greenland: Interpretation. *Science,* **246,** 1589–1591.

——, A. C. Brenner, J. A. Major, R. A. Bindschadler, and J. G. Marsh, 1989: Growth of Greenland: Measurement. *Science,* **246,** 1587–1589.

——, ——, ——, ——, and ——, 1990: Reply to Douglas et al. (1990). *Science,* **248,** 288–289.